

Black hole initial data in Gauss-Bonnet gravity: Momentarily static case

Hiroataka Yoshino

Cosmophysics Group, Institute of Particles and Nuclear Studies,

KEK, Tsukuba, Ibaraki, 305-0801, Japan

(Dated: February 8, 2011)

Abstract

We study the method for generating the initial data of black hole systems in Gauss-Bonnet (GB) gravity. The initial data are assumed to be momentarily static and conformally flat. Although the equation for the conformal factor is highly nonlinear, it is successfully solved by numerical relaxation for one-black-hole and two-black-hole systems. The common apparent horizon is studied in the two-black-hole initial data, and the result suggests that the Penrose inequalities are satisfied in this system. This is the first step for simulating black hole collisions in higher-curvature theories.

PACS numbers: 04.50.-h, 04.25.dg, 04.25.D-

I. INTRODUCTION

Higher-dimensional gravity has been attracting a lot of attentions motivated by the TeV-gravity scenarios [1–3]. If the three-dimensional space is a 3-brane in large or warped extra dimensions, the Planck energy could be of $O(\text{TeV})$, and the trans-Planckian collision will happen at accelerators such as the Large Hadron Collider (LHC) [4–6]. If this is the case, the intermediate state of a collision with sufficiently high energy and small impact parameter is expected to be a mini black hole, and this motivated a lot of works (see [7] for a review). At this time, no evidence for black hole signals has been found, and the restrictions for the Planck energy and the minimum black hole mass $M_{\text{BH}}^{(\text{min})}$ (such that the produced object can be regarded as a black hole if $M > M_{\text{BH}}^{(\text{min})}$) have been derived [8]. Another motivation for studying higher-dimensional gravity is the AdS/CFT correspondence, which conjectures the duality between gravity in anti-de Sitter (AdS) spacetime and the conformal field theory (CFT) on the boundary of that spacetime. If this conjecture is correct, the phenomena in CFT for which direct calculation is difficult due to strong coupling effect can be predicted by calculating the dual gravitational system.

One of the important approaches for higher-dimensional gravity is to explore the nonlinear dynamics of higher-dimensional spacetimes by numerical relativity. Several formulations and codes of higher-dimensional numerical relativity have been developed so far [9–11], and interesting simulations have been performed: the time evolution of Gregory-Laflamme instability [12], slow-velocity collision of black holes [10, 13, 14], dynamics of complex scalar field minimally coupled to gravity in Kaluza-Klein spacetimes [11], and bar-mode instability of rapidly rotating Myers-Perry black holes [15, 16]. In these works, time evolutions of spacetimes are simulated in the framework of general relativity (GR), which is the simplest theory of higher-dimensional gravity.

One of the interesting extensions of higher-dimensional numerical relativity is to include the higher-curvature terms. In four dimensions, the Lagrangian density that leads to the second-order equation of the metric is just the Ricci scalar. However, in higher-dimensions, the Lagrangian density including higher-curvature terms also leads to the second-order equation if the combination of higher-curvature terms are chosen appropriately. These theories are Gauss-Bonnet (GB) gravity [17] or, more generally, Lovelock gravity [18]. Among these higher-curvature theories, we take attention to GB gravity in this paper. The GB term gives

a quadratic correction with respect to the Riemann tensor to GR, and this GB correction arises in the low-energy limit of the heterotic string theory [19–21]. Therefore, the GB term may have important effects on the mini black hole phenomena at accelerators. Also, the AdS/CFT correspondence in the context of GB gravity has been considered (e.g., [22–24]).

The black holes in GB gravity have interesting properties. Although some part of GB gravity resembles GR, the other part does not. For example, the solution of a static spherically symmetric black hole found in Ref. [25] has two branches: the non-GR branch that is asymptotically AdS and the GR branch that is asymptotically flat (see [26, 27] for a detailed study on causal structures of these solution). The GB version of Birkoff’s theorem [28, 29] (see also [30] for Lovelock gravity) states that the spherically-symmetric vacuum spacetime (at least locally) corresponds to one of the two branches. The black hole of GR branch is shown to be unstable for $D = 5$ against scalar mode and for $D = 6$ against tensor mode if the coupling constant α_{GB} of the higher-curvature term is sufficiently larger than appropriate power of GM , where G is the gravitational constant and M is the Arnowitt-Deser-Misner (ADM) mass of the black hole [31–34] (see also [35] for a study that proves the generic appearance of instability of a spherically-symmetric black hole in Lovelock gravity).

The GB version of numerical relativity (say, numerical GB gravity), if it is developed, would play important roles to explore nonlinear phenomena in GB gravity. For example, the temporal evolution of the instability of a small spherically symmetric black hole could be followed by simulations to clarify the final end state. Also, by simulating the time evolution from initial data of a nonstationary rotating black hole, it would be possible to obtain an indication for the stationary rotating black holes whose analytic solutions have not been found to date (but see [36] for a numerical construction of the black hole with two equal rotational parameters). Of course, the simulation of high-velocity collision of black holes is an interesting issue to clarify the effect of higher-curvature terms on mini black hole phenomena at accelerators (see [37] for a partial result for a head-on collision of the Aichelburg-Sexl particles in GB gravity).

There are few studies for numerical GB gravity. The $N + 1$ formalism, which is the extension of the ADM formalism to GB gravity, has been done by Torii and Shinkai [38]. Similarly to the ADM formalism, Einstein-Gauss-Bonnet equation is decomposed into the Hamiltonian and momentum constraints and the evolution equations. On the other hand, the numerically stable formalism of GB gravity which is analogous to, e.g., Baumgarte-

Shapiro-Shibata-Nakamura (BSSN) formalism [39, 40] has not been developed yet, and also, no simulation of numerical GB gravity has been done.

When one simulates a spacetime in GB gravity, similarly to the case of GR, the first step is to prepare an initial spacelike hypersurface (i.e., initial data) by solving the constraint equations. In this paper, we focus attention to the method for preparing initial data of black hole systems in GB gravity. As a first step, the initial data are assumed to be momentarily static (i.e., time symmetric). In GR, the Brill-Lindquist initial data [41] are well known and widely used as the initial data of momentarily static multi black holes (see also [42, 43] for higher-dimensional studies). We discuss the extension of the Brill-Lindquist initial data to GB gravity, and successfully generate the initial data for one black hole and two equal-mass black holes.

Using the two-black-hole initial data, we discuss whether the Penrose inequality [44] holds in this system. The Penrose inequality states that the area of an apparent horizon (AH) is not greater than that of the Schwarzschild-Tangherlini black hole with the same ADM mass. In the case of the momentarily static initial data, the Penrose inequality was proved for $4 \leq D \leq 7$ using the conformal flow method [45]. It is of interest whether such a bound on the AH area holds or not in GB gravity. In addition to the original Penrose inequality, we also discuss whether the AH area is bounded from above by that of the spherically-symmetric black hole in GB gravity. The results suggest that both of the inequalities are held in this system.

This paper is organized as follows. In the next section, we review GB gravity and $N + 1$ formalism in this theory focusing attention to the part that is related to our study. In Sec. III, general framework for constructing the GB version of the Brill-Lindquist initial data is explained. The equation for the conformal factor Ψ is a Laplace equation with formal source term which is highly nonlinear in Ψ , and we prove the regularity of the source term which is necessary for the existence of the solution. In Sec. IV, the one-black-hole initial data are constructed numerically, and we show the agreement of the data with the time-symmetric slice of a spherically symmetric black hole spacetime. In Sec. V, the two-black-hole initial data are constructed. Using those data, we analyze the condition for the AH formation, and the Penrose inequalities in this system are discussed. Sec. VI is devoted to summary and discussion. Throughout this paper, we use the unit $c = 1$, while the gravitational constant G is explicitly written.

II. CONSTRAINT EQUATIONS IN GAUSS-BONNET GRAVITY

In this section, we review GB gravity and the $N + 1$ formalism of Ref. [38] focusing attention to the part that is related to the setup of our study.

A. Gauss-Bonnet action and equations

In this paper, D denotes the dimensionality of the spacetime \mathcal{M} with the metric $g_{\mu\nu}$. We also introduce $N = D - 1$, which is the dimensionality of a spacelike hypersurface Σ in the spacetime \mathcal{M} . Throughout this paper, we assume the spacetime to be vacuum. The Einstein-Gauss-Bonnet action [17] in D -dimensional spacetime is

$$S = \frac{1}{16\pi G} \int_{\mathcal{M}} (\mathcal{R} + \alpha_{\text{GB}} \mathcal{L}_{\text{GB}}) \sqrt{-g} d^D x \quad (1)$$

with

$$\mathcal{L}_{\text{GB}} = \mathcal{R}^2 - 4\mathcal{R}_{\mu\nu}\mathcal{R}^{\mu\nu} + \mathcal{R}_{\mu\nu\rho\sigma}\mathcal{R}^{\mu\nu\rho\sigma}, \quad (2)$$

where \mathcal{R} , $\mathcal{R}_{\mu\nu}$, and $\mathcal{R}_{\mu\nu\rho\sigma}$ are the Ricci scalar, the Ricci tensor, and the Riemann tensor, respectively, and α_{GB} is the coupling constant with dimensionality of squared length. The action (1) gives the gravitational equation as

$$\mathcal{G}_{\mu\nu} + \alpha_{\text{GB}} \mathcal{H}_{\mu\nu} = 0, \quad (3)$$

where

$$\mathcal{G}_{\mu\nu} = \mathcal{R}_{\mu\nu} - \frac{1}{2}\mathcal{R}g_{\mu\nu}, \quad (4)$$

and

$$\mathcal{H}_{\mu\nu} = 2(\mathcal{R}\mathcal{R}_{\mu\nu} - 2\mathcal{R}_{\mu\alpha}\mathcal{R}^{\alpha}_{\nu} - 2\mathcal{R}^{\alpha\beta}\mathcal{R}_{\mu\alpha\nu\beta} + \mathcal{R}_{\mu}^{\alpha\beta\gamma}\mathcal{R}_{\nu\alpha\beta\gamma}) - \frac{1}{2}g_{\mu\nu}\mathcal{L}_{\text{GB}}. \quad (5)$$

In the case $D = 4$, the term \mathcal{L}_{GB} in the action (1) gives a topological invariant as proved in the generalized Gauss-Bonnet theorem [46], and hence $\mathcal{H}_{\mu\nu} = 0$. The GB term becomes nontrivial only for higher dimensions, $D \geq 5$.

B. The $N + 1$ formalism

Here, we review the initial value equations in GB gravity based on the $N + 1$ formalism developed in Ref. [38]. We consider the spacelike hypersurface Σ with the induced metric

$\gamma_{\mu\nu}$ and the extrinsic curvature $K_{\mu\nu}$, and let n^μ be the future-directed timelike unit normal to the hypersurface. The projections of the gravitational equation $(\mathcal{G}_{\mu\nu} + \alpha_{\text{GB}}\mathcal{H}_{\mu\nu})n^\mu n^\nu$, $(\mathcal{G}_{\mu\nu} + \alpha_{\text{GB}}\mathcal{H}_{\mu\nu})n^\mu \gamma^\nu_\rho$, $(\mathcal{G}_{\mu\nu} + \alpha_{\text{GB}}\mathcal{H}_{\mu\nu})\gamma^\mu_\rho \gamma^\nu_\sigma$ give the Hamiltonian constraint, the momentum constraint, and the evolution equations, respectively. The initial data should be prepared so that they satisfy the two constraints. The Hamiltonian constraint is written as

$$M + \alpha_{\text{GB}}(M^2 - 4M_{ab}M^{ab} + M_{abcd}M^{abcd}) = 0, \quad (6)$$

where

$$M_{ijkl} = R_{ijkl} + (K_{ik}K_{jl} - K_{il}K_{jk}), \quad (7)$$

and $M_{ij} = \gamma^{ab}M_{iajb}$ and $M = \gamma^{ab}M_{ab}$. The explicit form of the other equations can be found in Ref. [38].

C. Conformal approach

Hereafter, we focus our attention to the momentarily static case, or in other words, the time-symmetric case: $K_{ij} = 0$. In this case, the momentum constraint is trivially satisfied, and $M_{ijkl} = R_{ijkl}$. We further assume the initial space Σ to be conformally flat:

$$\gamma_{ij} = \Psi^{4/(N-2)}\hat{\gamma}_{ij}, \quad (8)$$

where $\hat{\gamma}_{ij}$ is the flat-space metric. Note that the authors of Ref. [38] treated $\hat{\gamma}_{ij}$ as an arbitrary metric, and here we chose the very special case. Also, in Ref. [38], the conformal factor was set to be Ψ^{2m} , where m is an arbitrary number. Here $m = 2/(N - 2)$ is chosen, because in this case, we can treat the problem as a natural generalization of the GR studies.

In this setup, the equation for the conformal factor is written as

$$\hat{D}_a \hat{D}^a \Psi = \alpha_{\text{GB}} \hat{S}, \quad (9)$$

where \hat{D}_a is the covariant derivative with respect to the flat-space metric. Here, \hat{S} is written as

$$\hat{S} = \frac{N-3}{(N-1)(N-2)} \Psi^{-\frac{N+2}{N-2}} \left\{ 4(N-2) \left[(\hat{D}_a \hat{D}^a \Psi)^2 - (\hat{D}_a \hat{D}_b \Psi)(\hat{D}^a \hat{D}^b \Psi) \right] - 8\Psi^{-1}(\hat{D}\Psi)^2 \hat{D}_a \hat{D}^a \Psi + 8N\Psi^{-1} \hat{D}^a \Psi \hat{D}^b \Psi \hat{D}_a \hat{D}_b \Psi - \frac{4N(N-1)}{N-2} \Psi^{-2} (\hat{D}\Psi)^4 \right\}. \quad (10)$$

III. METHOD OF INITIAL DATA CONSTRUCTION

In this section, we give the formulation for generating the initial data with N_{BH} black holes in GB gravity.

A. Decomposition of conformal factor

Since we would like to obtain the initial data of GB gravity as continuous extension of those of the GR case, we decompose Ψ as

$$\Psi = \Psi_0 + \alpha_{\text{GB}}g. \quad (11)$$

Here, Ψ_0 is the solution in the GR case (i.e., $\hat{D}_a\hat{D}^a\Psi_0 = 0$), and the term $\alpha_{\text{GB}}g$ represents the deviation from the GR case in the presence of $\alpha_{\text{GB}} \neq 0$. The equation for g becomes

$$\hat{D}_a\hat{D}^ag = \hat{S} \quad (12)$$

with

$$\hat{S} = \frac{N-3}{(N-1)(N-2)}\Psi^{-\frac{N+2}{N-2}}\sum_{n=0}^4\alpha_{\text{GB}}^n s^{(n)}, \quad (13)$$

where

$$s^{(0)} = -4(N-2)(\hat{D}_a\hat{D}_b\Psi_0)(\hat{D}^a\hat{D}^b\Psi_0) + 8N\Psi^{-1}(\hat{D}_a\Psi_0)(\hat{D}_b\Psi_0)(\hat{D}^a\hat{D}^b\Psi_0) - \frac{4N(N-1)}{N-2}\Psi^{-2}(\hat{D}\Psi_0)^4, \quad (14)$$

$$s^{(1)} = -8(N-2)(\hat{D}_a\hat{D}_b\Psi_0)(\hat{D}^a\hat{D}^bg) - 8\Psi^{-1}(\hat{D}\Psi_0)^2(\hat{D}_a\hat{D}^ag) + 8N\Psi^{-1}\left[(\hat{D}_a\Psi_0)(\hat{D}_b\Psi_0)(\hat{D}^a\hat{D}^bg) + 2(\hat{D}^a\Psi_0)(\hat{D}^bg)(\hat{D}_a\hat{D}_b\Psi_0)\right] - \frac{16N(N-1)}{N-2}\Psi^{-2}(\hat{D}\Psi_0)^2(\hat{D}_a\Psi_0)(\hat{D}^ag), \quad (15)$$

$$s^{(2)} = -4(N-2)\left[(\hat{D}_a\hat{D}_bg)(\hat{D}^a\hat{D}^bg) - (\hat{D}^a\hat{D}^ag)^2\right] - 16\Psi^{-1}(\hat{D}_a\Psi_0)(\hat{D}^ag)(\hat{D}^b\hat{D}_bg) + 8N\Psi^{-1}\left[(\hat{D}^ag)(\hat{D}^bg)(\hat{D}_a\hat{D}_b\Psi_0) + 2(\hat{D}^a\Psi_0)(\hat{D}^bg)(\hat{D}_a\hat{D}_bg)\right] - \frac{8N(N-1)}{N-2}\Psi^{-2}\left[2(\hat{D}_a\Psi_0\hat{D}^ag)^2 + (\hat{D}\Psi_0)^2(\hat{D}g)^2\right], \quad (16)$$

$$s^{(3)} = -8\Psi^{-1}(\hat{D}g)^2(\hat{D}^a\hat{D}_ag) + 8N\Psi^{-1}(\hat{D}^ag)(\hat{D}^bg)(\hat{D}_a\hat{D}_bg) - \frac{16N(N-1)}{N-2}\Psi^{-2}(\hat{D}_a\Psi_0)(\hat{D}^ag)(\hat{D}g)^2, \quad (17)$$

and

$$s^{(4)} = -\frac{4N(N-1)}{N-2}\Psi^{-2}(\hat{D}g)^4. \quad (18)$$

We call the right hand side \hat{S} of Eq. (12) the ‘‘source term’’ hereafter.

B. Puncture initial data

Here, we specify the GR solution Ψ_0 of a system with N_{BH} black holes. For this purpose, we introduce the Cartesian coordinates (x^a) to the flat space and specify N_{BH} points at which Ψ_0 diverges (i.e., punctures). The location of the n -th puncture is denoted by $x^a = \bar{x}_{(n)}^a$, and we define $x_{(n)}^a = x^a - \bar{x}_{(n)}^a$ and $R_{(n)} = |x_{(n)}^a|$. Then, the solution to the Laplace equation $\hat{D}_a\hat{D}^a\Psi_0 = 0$ is adopted as

$$\Psi_0 = 1 + \sum_{n=1}^{N_{\text{BH}}} \psi_{(n)}, \quad (19)$$

with

$$\psi_{(n)} = \frac{4\pi GM_0^{(n)}}{(N-1)\Omega_{N-1}R_{(n)}^{N-2}}, \quad (20)$$

where Ω_{N-1} denotes the area of a $(N-1)$ -dimensional unit sphere and $M_0^{(n)}$ is a mass parameter for n -th black hole. The Arnowitt-Deser-Misner (ADM) mass M_0 is given as $M_0 = \sum_{n=1}^{N_{\text{BH}}} M_0^{(n)}$. This solution was studied in Ref. [41] in the $D = 4$ case and is often called the Brill-Lindquist initial data (see [42, 43] for the studies in higher-dimensional cases). This space possesses the N_{BH} Einstein-Rosen bridges (say, throats) and each puncture corresponds to the asymptotically flat region beyond each throat.

C. Finiteness of the source term

The conformal factor Ψ_0 of the Brill-Lindquist initial data in the GR case diverges at each puncture as $R_{(n)}^{-(N-2)}$. Then, a naive estimate gives a severely divergent behavior of the source term $\hat{S} \sim R_{(n)}^{-(N+4)}$ at each puncture. If this is the case, g also has to diverge at each puncture, and then, the behavior of \hat{S} would be further modified, implying further stronger

divergence of g . This procedure would continue eternally, and hence the solution g would not exist.

However, this naive estimate is not correct, since the cancellation of divergent terms occurs. As a result, \hat{S} becomes zero at the punctures, and hence the source term \hat{S} is well behaved. Let us check this in the following.

Assuming a regular behavior of g at each puncture, the functions $s^{(2)}$, $s^{(3)}$, and $s^{(4)}$ obviously become zero at each puncture after multiplying the factor $\Psi^{-(N+2)/(N-2)}$ in Eq. (13). Therefore, we focus our attention only to $s^{(0)}$ and $s^{(1)}$. We substitute Eq. (19) into Eqs. (14) and (15), rewrite it with $R_{(n)}\psi''_{(n)} + (N-1)\psi'_{(n)} = 0$, and collect only terms for which divergence at the punctures is suspected. For example, $\Psi^{-2}(D\Psi_0)^4$ from the third term of Eq. (14) is calculated as

$$\begin{aligned}\Psi^{-2}(D\Psi_0)^4 &= \Psi^{-2} \sum_{k,l,m,n} \psi'_{(k)}\psi'_{(l)}\psi'_{(m)}\psi'_{(n)}(\vec{n}_{(k)} \cdot \vec{n}_{(l)})(\vec{n}_{(m)} \cdot \vec{n}_{(n)}) \\ &= \Psi^{-2} \left[\sum_k \psi'^4_{(k)} + 4 \sum_{k,l(k \neq l)} \psi'_{(k)}\psi'^3_{(l)}(\vec{n}_{(k)} \cdot \vec{n}_{(l)}) + O(\psi'^2) \right],\end{aligned}\quad (21)$$

where $n^a_{(n)} = x^a_{(n)}/R_{(n)}$ is the unit vector and $(\vec{n}_{(k)} \cdot \vec{n}_{(l)})$ is the inner product. Here, $O(\psi'^2)$ are the terms that become zero at the punctures after multiplying the factor $\Psi^{-(N+2)/(N-2)}$ in Eq. (13), and thus, we do not consider these terms because we are interested in cancellation of divergent terms. In this manner, $s^{(0)}$ and $s^{(1)}$ are calculated as

$$\begin{aligned}s^{(0)} &= -\frac{4N(N-1)}{N-2} \sum_k \left(\frac{\psi'_{(k)}}{R_{(k)}\Psi} \right)^2 [R_{(k)}\psi'_{(k)} + (N-2)\Psi]^2 \\ &\quad + 4N \sum_{k,l(k \neq l)} \frac{\psi'_{(k)}\psi'_{(l)}}{\Psi} \left\{ [R_{(k)}\psi'_{(k)} + R_{(l)}\psi'_{(l)} + (N-2)\Psi] \frac{1 - N(\vec{n}_{(k)} \cdot \vec{n}_{(l)})^2}{R_{(k)}R_{(l)}} \right. \\ &\quad \left. - \frac{4(N-1)}{N-2} \left(\frac{\psi'_{(l)}}{\Psi} \right) [R_{(l)}\psi'_{(l)} + (N-2)\Psi] \frac{(\vec{n}_{(k)} \cdot \vec{n}_{(l)})}{R_{(l)}} \right\} + O(R_{(k)}^{-2}),\end{aligned}\quad (22)$$

$$\begin{aligned}s^{(1)} &= -8 \sum_k [R_{(k)}\psi'_{(k)} + (N-2)\Psi] \left(\frac{\psi'_{(k)}}{R_{(k)}\Psi} \right) \\ &\quad \times \left[\hat{D}^a \hat{D}_a g + N n^a_{(k)} n^b_{(k)} \hat{D}_b \hat{D}_a g + \frac{2N(N-1)}{N-2} \left(\frac{\psi'_{(k)}}{\Psi} \right) n^a_{(k)} \hat{D}_a g \right] + O(R_{(k)}^{-2}).\end{aligned}\quad (23)$$

Now, we use the relation

$$R_{(n)}\psi'_{(n)} + (N-2)\psi_{(n)} = 0. \quad (24)$$

and find $s^{(0)} = O(R_{(n)}^{-4})$ and $s^{(1)} = O(R_{(n)}^{-3})$. Therefore, \hat{S} behaves as $\sim R_{(n)}^{N-2}$ at each puncture, and no divergence of the source term occurs. For this reason, we can expect the existence of the solution of g that is regular at each puncture.

In Secs. IV and V, we explicitly construct the numerical solution of g for one black hole and two black holes, respectively, assuming the regularity of g at each puncture. There, it turns out that this numerical method works well. It is worth pointing out the relation between our method and the method for generating non-time-symmetric initial data of puncture-type boosted black holes in GR developed by Brandt and Brügmann [47]. In their formalism, the space is assumed to be conformally flat, and the analytic solution of the extrinsic curvature found by Bowen and York [48] is used. The conformal factor is decomposed as $\Psi = \Psi_0 + \psi$, where Ψ_0 is the conformal factor for the Brill-Lindquist solution. The equation for ψ becomes the Laplace equation with a formal source term depending on Ψ . Here, the source term is shown to become zero at each puncture, and hence, ψ can be solved numerically assuming the regularity at each puncture. Therefore, our method is very analogous to the Brandt-Brügmann formalism.

D. ADM mass

Here, we discuss how to calculate the total gravitational energy. The ADM mass M is given by

$$M = -\frac{(N-1)}{4\pi(N-2)G} \int_{\mathcal{S}} \hat{D}_a \Psi dS^a, \quad (25)$$

where \mathcal{S} is the surface at infinity. Suppose $\Psi = \Psi_0$ is the conformal factor with the ADM mass M_0 in the GR case. Then, using the Gauss law and Eq. (12), we find that the ADM mass in the GB case is

$$M = M_0 - \frac{(N-1)\alpha_{\text{GB}}}{4\pi(N-2)G} \int_{\hat{\Sigma}} \hat{S} dx_1 \dots dx_N, \quad (26)$$

where $\hat{\Sigma}$ is the whole flat space. It is important to point out that the ADM mass M in the case $\alpha_{\text{GB}} \neq 0$ is different from M_0 , although M_0 is the ADM mass in the GR case $\alpha_{\text{GB}} = 0$. Therefore the parameter M_0 is (say) an artificial mass for $\alpha_{\text{GB}} \neq 0$, and the true ADM mass M is determined after Ψ is solved. The similar phenomena can be found also in the Brandt-Brügmann formalism.

IV. ONE-BLACK-HOLE INITIAL DATA

Let us begin our numerical analysis with the one-black-hole initial data. Here we assume the initial data to be spherically symmetric and introduce the radial coordinate R in which the metric of the flat space becomes

$$ds^2 = dR^2 + R^2 d\Omega_{N-1}^2. \quad (27)$$

Here, $d\Omega_{N-1}^2$ is the line element of the $(N-1)$ -dimensional unit sphere. We impose $g = g(R)$ and set the function Ψ_0 in Eq. (11) to be

$$\Psi_0 = 1 + \left(\frac{R_S(M_0)}{R} \right)^{N-2}, \quad (28)$$

where we defined $R_S(M_0)$ as

$$R_S(M_0) := \left[\frac{4\pi G M_0}{(N-1)\Omega_{N-1}} \right]^{1/(N-2)}. \quad (29)$$

Note that $R_S(M_0)$ is different from the Schwarzschild radius $r_S(M_0)$, and they are related as $r_S(M_0) = 4^{1/(N-2)} R_S(M_0)$.

In the case of $\alpha_{\text{GB}} = 0$, the conformal factor $\Psi = \Psi_0$ gives the spacelike hypersurface which is known as the Einstein-Rosen bridge (i.e., the time-symmetric Cauchy slice in the Schwarzschild-Tangherlini spacetime). The coordinate R is called the isotropic coordinate, and the minimal surface (or the apparent/event horizon) is located at $R = R_S(M_0)$. Because of the GB version of Birkoff's theorem [28, 29], also in the case of $\alpha_{\text{GB}} > 0$, the initial data is expected to give the time-symmetric Cauchy slice of the spherically-symmetric black hole spacetime [25] whose metric is

$$ds^2 = -f(r)dt^2 + \frac{dr^2}{f(r)} + r^2 d\Omega_{N-1}^2, \quad (30)$$

with

$$f(r) = 1 + \frac{r^2}{2\tilde{\alpha}_{\text{GB}}} \left(1 - \sqrt{1 + \frac{4\tilde{\alpha}_{\text{GB}}\tilde{M}}{r^N}} \right), \quad (31)$$

where $\tilde{\alpha}_{\text{GB}} = (N-2)(N-3)\alpha_{\text{GB}}$ and $\tilde{M} = [r_S(M)]^{N-2}$. If we can find the coordinate transformation from the Schwarzschild-like coordinate r to the isotropic coordinate R , the conformal factor $\Psi(R)$ is obtained. However, since $f(r)$ has a complicated form in the cases $\alpha_{\text{GB}} \neq 0$, it seems impossible to find the analytic formula for the coordinate transformation

in contrast to the GR case. Therefore, this problem has to be solved numerically. Besides, we can obtain a lot of lessons for the numerical method from this problem as we will see later.

A. Perturbative analysis

In the numerical calculation, $R_S(M_0)$ is adopted as the unit of the length, and also in the following, we use the unit $R_S(M_0) = 1$ unless explicitly specified. Let us consider the case where the coupling constant α_{GB} is small, and thus, the correction from the GR case can be treated as a perturbation. In this case, Ψ in Eq. (12) should be replaced by Ψ_0 , and the equation is reduced to

$$g_{,RR} + \frac{N-1}{R}g_{,R} = -4N(N-3)R^{-2}\Psi_{0,R}^2\Psi_0^{-3-\frac{4}{N-2}}. \quad (32)$$

Here, the cancellation of divergent terms has occurred in the right-hand side because of the relation $\Psi_{0,R} + (N-2)\Psi_0/R = (N-2)/R$, and as a result, the source term is $O(R^{N-2})$ in the neighborhood of the puncture. In the case of $D = 5$ (i.e., $N = 4$), this equation can be solved analytically:

$$g = \frac{4(1 + 3R^2 + R^4)}{3(1 + R^2)^3}. \quad (33)$$

Thus we explicitly confirm the existence of the solution that is regular at the origin $R = 0$. This result leads to the expectation that a regular solution of g exists in more general cases including higher-order terms in α_{GB} .

The function g behaves as $\simeq (4/3)R^{-2}$ at the distant region, $R \gg 1$. This indicates that the ADM mass is shifted as

$$M = M_0 + \frac{2\pi\alpha_{\text{GB}}}{G}. \quad (34)$$

Therefore, we confirm the statement of Sec. III D explicitly: If we impose the regularity of g at the origin, the function g also contributes to the mass, and hence, the ADM mass is determined after g is solved.

B. Numerical approach

Now, we study the numerical generation of $g(R)$ for the general cases of $\alpha_{\text{GB}} \geq 0$. We write down the Laplace operator $\hat{D}_a\hat{D}^a$ and the source term \hat{S} in terms of the radial coor-

dinate R . Here, we adopt the formulas of $s^{(0)}$ and $s^{(1)}$ for which the divergent terms are canceled out by the relation $\Psi_{0,R} + (N - 2)\Psi/R = (N - 2)(1 + \alpha_{\text{GB}}g)/R$. Then, the right hand side becomes $O(R^{N-2})$ similarly to the perturbative case and the source term \hat{S} is well behaved at the origin $R = 0$. This confirms the general proof for the finiteness of \hat{S} of Sec. III C.

The numerical calculation is done in a finite region, and hence, there is an outer boundary of the computation domain, $R = R_{\text{max}}$. Here, we have to specify the outer boundary condition. As discussed in the previous subsection, the behavior of g at $R \gg 1$ is expected to be $g \simeq C/R^{N-2}$. Since the value of C is not known before solving g , we eliminate C using the combination of $g_{,R}$ and g as

$$g_{,R} + (N - 2)g/R = 0, \quad (35)$$

and adopt this Robin boundary condition at $R = R_{\text{max}}$.

We used the finite differencing method with the fourth-order accuracy with respect to the grid size. Here, the method of nested hierarchical grids was adopted in the numerical calculation. Specifically, we located the outer boundary at $R_{\text{max}} = 1024$, and put 12 and 16 layers for $0 \leq \alpha_{\text{GB}} < 10^2$ and $10^2 \leq \alpha_{\text{GB}}$, respectively (remember that the unit of the length is $R_S(M_0)$). The boundary of the n -th layer is located at $R = 1024/2^{n-1}$, and the grid size is $12.8/2^{n-1}$. Then, the solutions were obtained by using the successive-over-relaxation (SOR) method: For each calculation, a test surface is prepared initially and it is made slowly converge to the real solution until the difference from the finite difference equations normalized by the absolute value of g becomes less than 10^{-12} .

Figure 1 shows the behavior of g as a function of R for $\alpha_{\text{GB}} = 0$ and 10^k for $D = 5-8$, where $k = 1, \dots, 4$ for $D = 5$ and 6 and $k = 1, \dots, 3$ for $D = 7$ and 8. The curve for $\alpha_{\text{GB}} = 0$ in the case $D = 5$ agrees with Eq. (33). As α_{GB} is increased, the curve becomes steeper around the origin. This is the reason why we increased the number of the layers for $100 \leq \alpha_{\text{GB}}$: More grid number is required for larger α_{GB} .

In order to check that the geometry of the generated initial data agrees with that of the time-symmetric Cauchy surface in the spherically-symmetric spacetime, Eqs. (30) and (31), we calculate the minimal surface (or the AH) and compare the relations between the two nondimensional quantities, $\alpha_{\text{GB}}/r_S^2(M)$ and $r_H/r_S(M)$, where r_H is the horizon radius. The

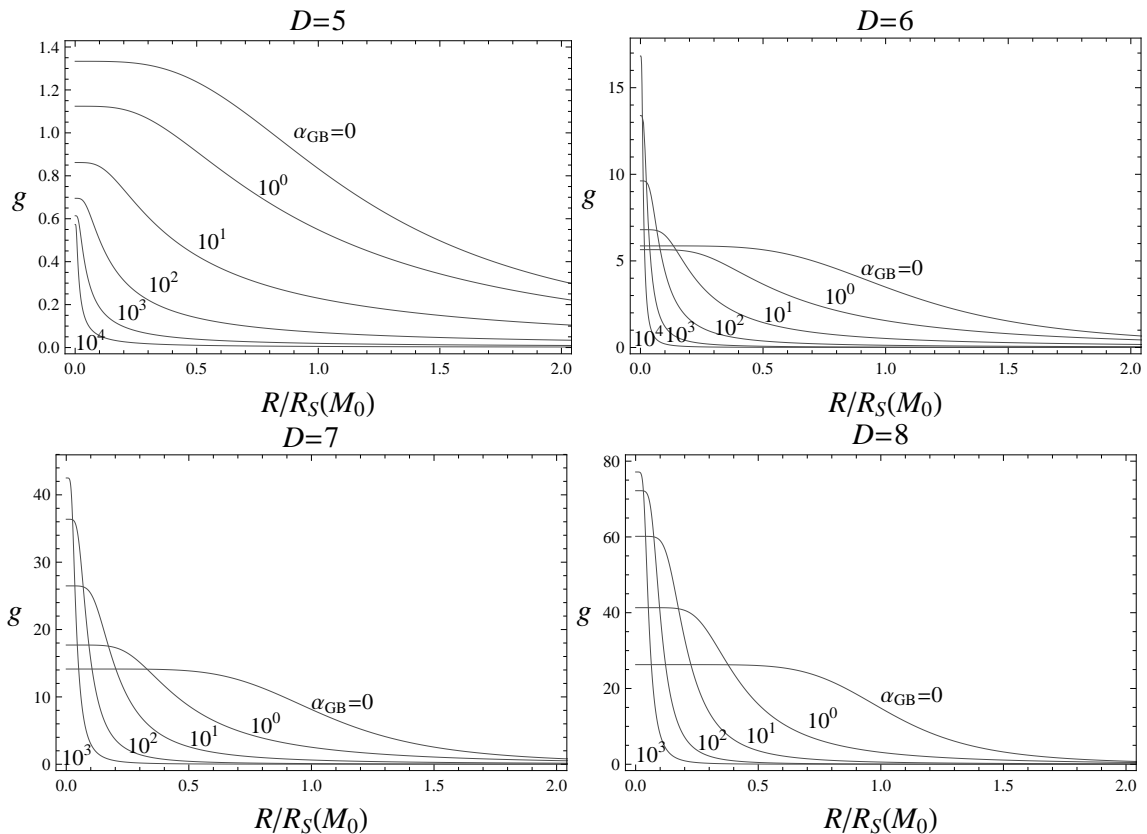


FIG. 1: The behavior of g (in the unit of $R_S^2(M_0)$) as functions of $R/R_S(M_0)$ for $D = 5, 6, 7,$ and 8 for the cases $\alpha = 0$ and 10^k with $0 \leq k \leq 3$. For $D = 5$ and 6 , the case $\alpha = 10^4$ is also shown.

horizon of the analytic solution is given by $f(r_H) = 0$, which leads to the relation

$$\left(\frac{r_H}{r_S}\right)^{N-4} \left[\left(\frac{r_H}{r_S}\right)^2 + \frac{\tilde{\alpha}_{\text{GB}}}{r_S^2} \right] = 1. \quad (36)$$

On the other hand, we find the minimal surface of the numerical data by searching the location $R = R_H$ at which

$$\frac{2}{N-2} R \Psi_{,R} + \Psi = 0 \quad (37)$$

is satisfied, and calculate the horizon radius as

$$r_H = R_H \Psi^{2/(N-2)}(R_H). \quad (38)$$

Then, the ADM mass M is calculated by Eq. (26), and the value of $r_H/r_S(M)$ is evaluated.

Figure 2 shows the relation between $\alpha_{\text{GB}}/r_S^2(M)$ and $r_H/r_S(M)$ for $D = 5-8$. The solid curve shows the analytic formula, and the circles are our numerical data points. They agree very well, and thus, we can confirm that the generated initial data is the time-symmetric

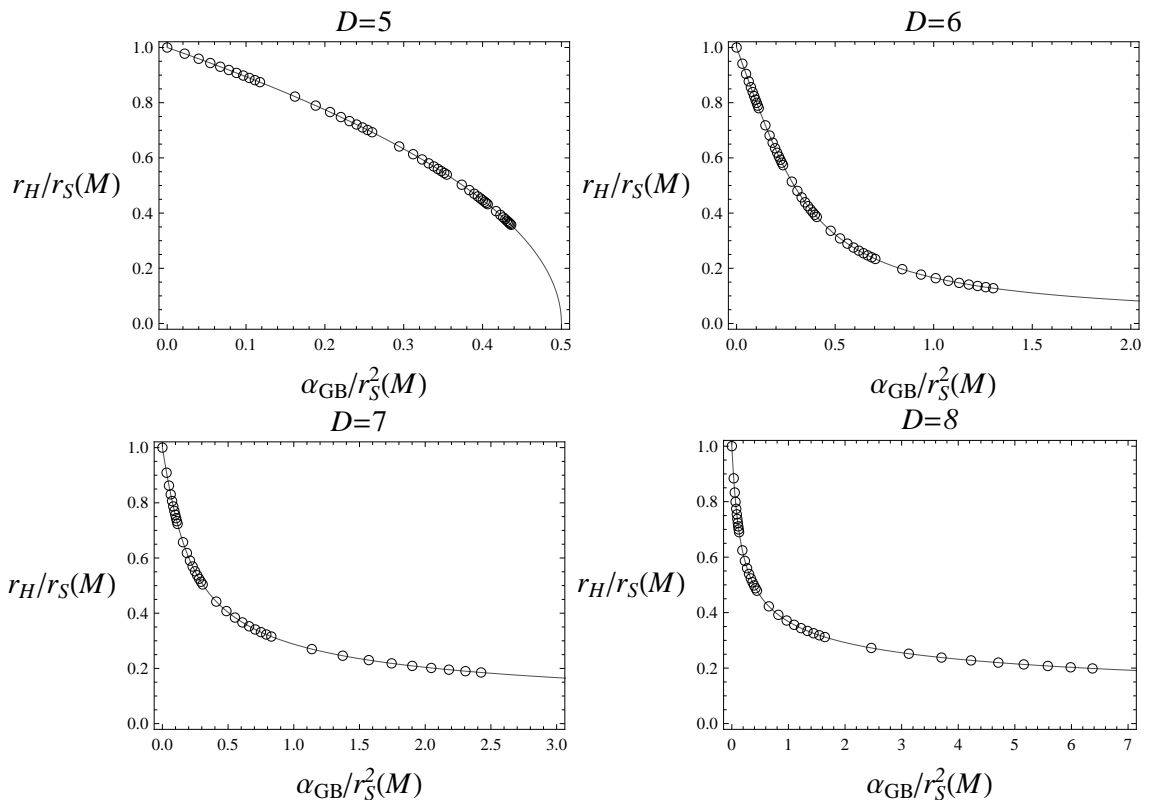


FIG. 2: The radius $r_H/r_S(M)$ of the minimal surface as a function of $\alpha_{\text{GB}}/r_S^2(M)$ for $D = 5, 6, 7,$ and 8 . Each straight curve shows the analytic relation, while the circles (\circ) show the numerical result. The numerical data are taken for $\alpha_{\text{GB}}/R_S^2(M_0) = 0, n \times 10^{k-1}$ (where n and k are integers satisfying $1 \leq n \leq 9$ and $0 \leq k \leq k_{\text{max}}$), and $10^{k_{\text{max}}}$, where $k_{\text{max}} = 4$ for $D = 5$ and 6 whereas $k_{\text{max}} = 3$ for $D = 7$ and 8 . The data agree well with the analytic relation.

slice in the spherically-symmetric spacetime. The cases for $\alpha_{\text{GB}}/R_S^2(M_0) = 0, n \times 10^{k-1}$ (where n and k are integers satisfying $1 \leq n \leq 9$ and $0 \leq k \leq k_{\text{max}}$), and $10^{k_{\text{max}}}$ are shown for all D . Here, k_{max} is chosen as $k_{\text{max}} = 4$ for $D = 5$ and 6 , and $k_{\text{max}} = 3$ for $D = 7$ and 8 . As seen from this figure, the value of $r_H/r_S(M)$ is decreased as $\alpha_{\text{GB}}/R_S^2(M_0)$ is increased, but even at $\alpha_{\text{GB}}/R_S^2(M_0) = 10^4$, the value of $r_H/r_S(M)$ is $\simeq 0.36$ and 0.13 for $D = 5$ and 6 , respectively. Therefore, generating the initial data with a horizon radius r_H that is much smaller than the Schwarzschild radius r_S requires a very large number of $\alpha_{\text{GB}}/R_S^2(M_0)$, and thus, it is a hard task at least in this approach.

Here, we point out the importance of the location of the outer boundary R_{max} . Figure 3 shows the numerical results with the choices of $R_{\text{max}} = 16$ and 64 . The agreement with the analytic relation is fairly good for small α_{GB} , but the deviation becomes significant for

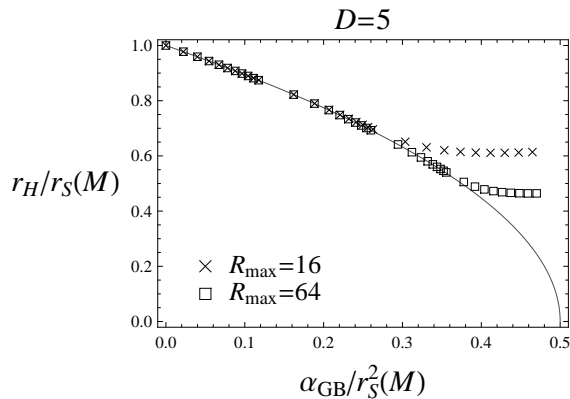


FIG. 3: The numerical data taken for $R_{\max} = 16$ (crosses, \times) and 64 (squares, \square) in the case of $D = 5$. The deviation from the analytic relation becomes significant for $\alpha_{\text{GB}}/R_S^2(M_0) \gtrsim 10$ and 100 for $R_{\max} = 16$ and 64, respectively, indicating that the larger number of R_{\max} is required for accurate numerical calculations as α_{GB} is increased.

$\alpha_{\text{GB}}/R_S^2(M_0) \gtrsim 10$ and 100 for $R_{\max} = 16$ and 64, respectively. This is because the integrand of Eq. (26) cannot be ignored for $R > R_{\max}$ and therefore the ADM mass M is evaluated to be a smaller value than the true value. We have to remember that the larger value of R_{\max} is required for a larger number of α_{GB} for accurate calculations.

Now we summarize the lessons obtained in the analysis in this section: (i) The source term for the equation g becomes zero at $R = 0$ because of the cancellation of divergent terms, and thus, the regular solution can be constructed; (ii) The ADM mass M has to be evaluated after the function g is generated, because it contributes to the mass; (iii) The function g becomes steeper around $R = 0$ as α_{GB} is increased, and therefore, the better resolution is required; and (iv) We have to take care of the location of the outer boundary R_{\max} for large α_{GB} values since the integrand of Eq. (26) becomes large at the distant region.

V. TWO-BLACK-HOLE INITIAL DATA

Now we turn our attention to the study on the two-black-hole initial data. After generating the conformal factor, we study the common AH and assess whether the Penrose-like inequalities are held in this system.

A. Numerical calculation

We assume the two black holes to have the same mass and the initial space to be axisymmetric with $O(N - 1)$ symmetry (i.e., there is the z -axis and the directions orthogonal to axis have the same structure). To be specific, we introduce the (z, ρ) coordinates where the metric of the flat space is

$$ds^2 = dz^2 + d\rho^2 + \rho^2 d\Omega_{N-2}^2, \quad (39)$$

and assume $\Psi = \Psi(z, \rho)$. The GR solution Ψ_0 is adopted as the Brill-Lindquist solution with two equal-mass black holes that is described as

$$\Psi_0 = 1 + \frac{1}{2}[R_S(M_0)]^{N-2} \left(\frac{1}{R_+^{N-2}} + \frac{1}{R_-^{N-2}} \right). \quad (40)$$

Here, the punctures are located at $z = \pm z_0$ on the z axis and

$$R_{\pm} := \sqrt{(z \mp z_0)^2 + \rho^2}, \quad (41)$$

and $R_S(M_0)$ is defined in Eq. (29). In this setup, the space possesses the two throats and three asymptotically flat regions (say, one upper sheet and two lower sheets). The input parameters in the numerical calculations are z_0 and α_{GB} in the unit $R_S(M_0) = 1$.

In the numerical calculation of $g(z, \rho)$, we write down the Laplace operator $\hat{D}_a \hat{D}^a$ and the source term \hat{S} in terms of (z, ρ) , where the divergent terms of Eqs. (14) and (15) (i.e., $s^{(0)}$ and $s^{(1)}$) are canceled out. Since the two black holes have the same mass, there is a mirror symmetry with respect to $z = 0$. For this reason, we choose the computation domain as $0 \leq z \leq z_0 + \Delta z_{\text{max}}$ and $0 \leq \rho \leq \Delta \rho_{\text{max}}$ where Δz_{max} and $\Delta \rho_{\text{max}}$ are chosen as $\Delta z_{\text{max}} = \Delta \rho_{\text{max}} = 1024$ in the unit $R_S(M_0) = 1$. At the outer boundary, we impose the same boundary condition (35) as the spherically symmetric case but rewritten in the (z, ρ) coordinates. Similarly to the case of one-black-hole initial data, we used the fourth-order finite differencing and the method of nested hierarchical grids. We put 13 layers to the computational domain, where the n -th layer has the boundary at $z = z_0 \pm \Delta z_{\text{max}}/2^{n-1}$ and $\rho = \Delta \rho_{\text{max}}/2^{n-1}$. If the layer crosses $z = 0$, the region $z < 0$ is discarded. The grid number N_{grid} of ρ coordinate of each layer is varied as 10, 20, and 40 depending on the situation, and the grids of z coordinate have the same size. Then, the solution is obtained by the SOR method. The relaxation is continued until the deviation from the finite difference equations normalized by the absolute value of g becomes less than 10^{-12} .

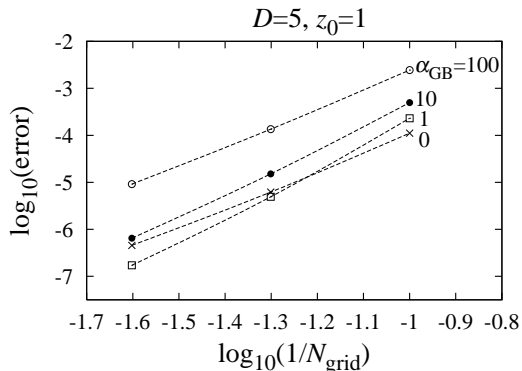


FIG. 4: Relation between numerical error in $g(z, \rho)$ and inverse of the grid number ($1/N_{\text{grid}}$) (proportional to the grid size) for $\alpha_{\text{GB}} = 0$ (\times), 1 (\square), 10 (\bullet), and 100 (\circ) for the case $D = 5$ and $z_0 = 1$.

The validity of the numerical computation is checked in three manners. First, it is checked that the numerical solution $g(z, \rho)$ in the case of $z_0 = 0$ agrees with that of one-black-hole initial data. Next, as z_0 is increased, the solution is expected to asymptote to that of one isolated black hole with half mass in the neighborhood of each puncture, and the numerical solution $g(z, \rho)$ is actually confirmed to show this behavior. Finally, we checked whether the numerical solution shows the appropriate convergence with respect to the grid size. Figure 4 shows the typical numerical error in $g(z, \rho)$ for $\alpha_{\text{GB}} = 0, 1, 10,$ and 100 for the case $D = 5$ and $z_0 = 1$ as a function of $\log_{10}(1/N_{\text{grid}})$. Here, the error is evaluated for $N_{\text{grid}} = 10, 20,$ and 40 by calculating the difference from the solution of the case $N_{\text{grid}} = 80$. The slope for the curves of $\alpha_{\text{GB}} = 0$ and 100 is approximately four, reflecting the fact that the adopted method is the fourth-order accuracy scheme. On the other hand, the slope for the curves of $\alpha = 1$ and 10 is larger than four; the slope for $\alpha = 1$ is approximately five. This is a somewhat strange result, because the five-order accuracy was obtained by using the scheme with the fourth-order accuracy. This is probably because the numerical error in g changes the value of the right-hand side \hat{S} of Eq. (12), and the change in \hat{S} further modify the value of g . Because of this effect, the cancellation of the numerical error would have happened accidentally. Anyway, the numerical data shows at least the fourth-order convergence, and this supports the accuracy of our numerical calculation.

Figure 5 shows the 3D plot of the generated data $g(z, \rho)$ for $z_0 = 1$ and $\alpha_{\text{GB}} = 0, 1,$ and 10 in the case $D = 5$. Here, the data of the ninth layer (layer of $n = 9$) are used to draw this

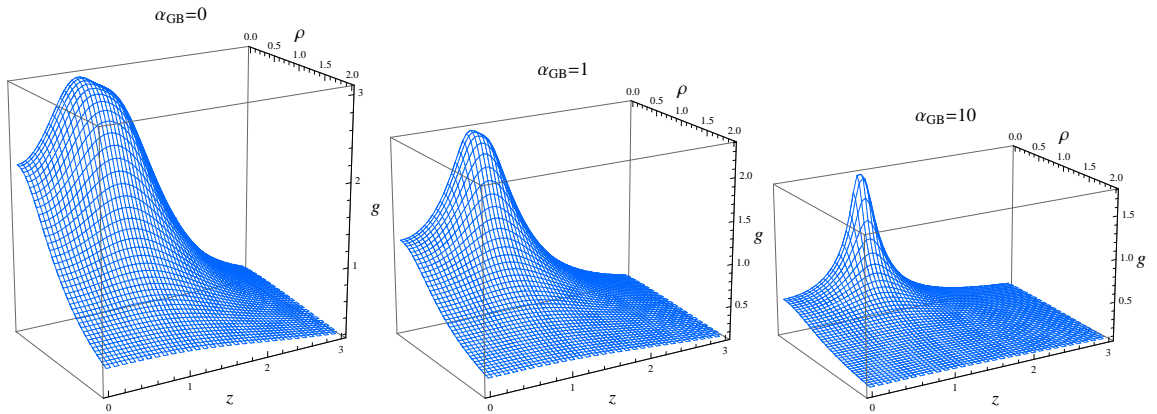


FIG. 5: 3D plot of the function $g(z, \rho)$ in the domain $0 \leq z \leq 3$ and $0 \leq \rho \leq 2$ in the case $z_0 = 1$ and $D = 5$. The cases for $\alpha_{\text{GB}} = 0$ (left), 1 (center), and 10 (right) are shown.

figure. As the value of α_{GB} is increased, the surface becomes steeper around the puncture.

B. Common apparent horizon

The AH is defined as the outermost marginally trapped surface, and it satisfies the equation of zero expansion, $\theta_+ = \nabla_\mu k^\mu = 0$, where k^μ is a tangent vector of the null geodesic congruence from the AH. In GR, the formation of an AH implies the existence of an event horizon (EH) outside of it assuming the cosmic censorship and the null energy condition for the energy-momentum tensor. On the other hand, in GB gravity, this statement does not hold because whether $-\mathcal{H}_{\mu\nu}$ obeys the null energy condition is quite uncertain. However, also in GB gravity, the formation of an AH at least implies the existence of a region where gravity is strong. Furthermore, many theorems, such as the area theorem and the second law for a future trapping horizon, has been shown to hold also in GB gravity for a spherically-symmetric system with matter of GR branch [49]. For this reason, the AH may imply the black hole formation also in GB in a certain condition. For this reason, it is interesting to study the formation of an AH also in GB gravity.

Because the space is momentarily static in our setup, the equation of an apparent horizon is reduced to $D_i s^i = 0$, where s^i is a unit normal to the horizon. Assuming the location of

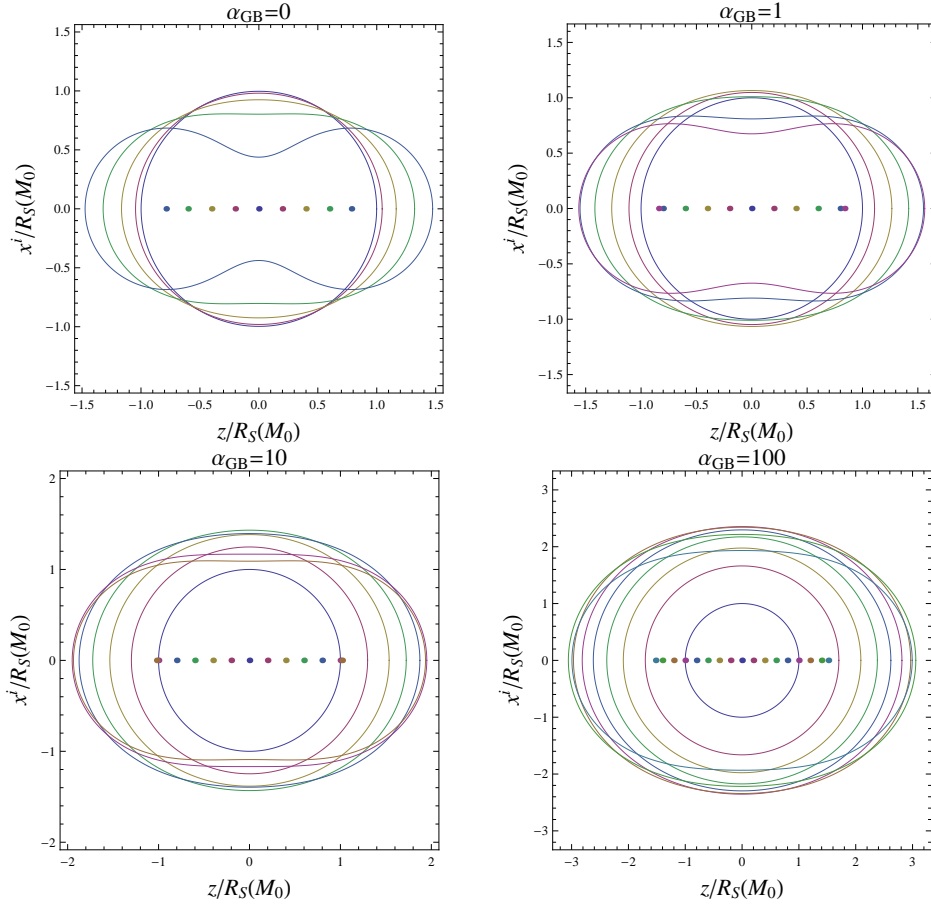


FIG. 6: Coordinate shapes of the AH on a (z, x^i) plane in the unit of $R_S(M_0) = 1$ in the case of $D = 5$ and $\alpha_{\text{GB}} = 0, 1, 10,$ and 100 . The cases for several values of z_0 are shown with 0.2 intervals starting from zero, and the case $z_0 = z_0^{(\text{crit})}$ is also shown. The location of the punctures are shown by dots. As z_0 is increased, the horizon becomes distorted.

the AH to be $R = h(\theta)$, where $\theta = \arctan(\rho/z)$, the horizon equation becomes

$$h_{,\theta\theta} - (D-2)(h^2 + h_{,\theta}^2) \left(\frac{2}{D-3} \frac{\Psi_{,R}}{\Psi} + \frac{1}{h} \right) + \frac{h_{,\theta}^2}{h} + h_{,\theta} \left(1 + \frac{h_{,\theta}^2}{h^2} \right) \left[\frac{2(D-2)}{(D-3)} \frac{\Psi_{,\theta}}{\Psi} + (D-3) \cot \theta \right] = 0. \quad (42)$$

The common AH that encloses the two black holes is found using the so-called shooting method by solving this equation under the boundary condition $h_{,\theta} = 0$ at $\theta = 0$ and $\pi/2$.

Figure 6 shows examples of coordinate shape of the common AH on the (z, x^i) plane, where x^i is one of the orthogonal directions to the z axis. Here, the cases $D = 5$ and $\alpha_{\text{GB}} = 0, 1, 10,$ and 100 are shown, and the values of z_0 are $0, 0.2, \dots,$ and $z_0^{(\text{crit})}$, where $z_0^{(\text{crit})}$

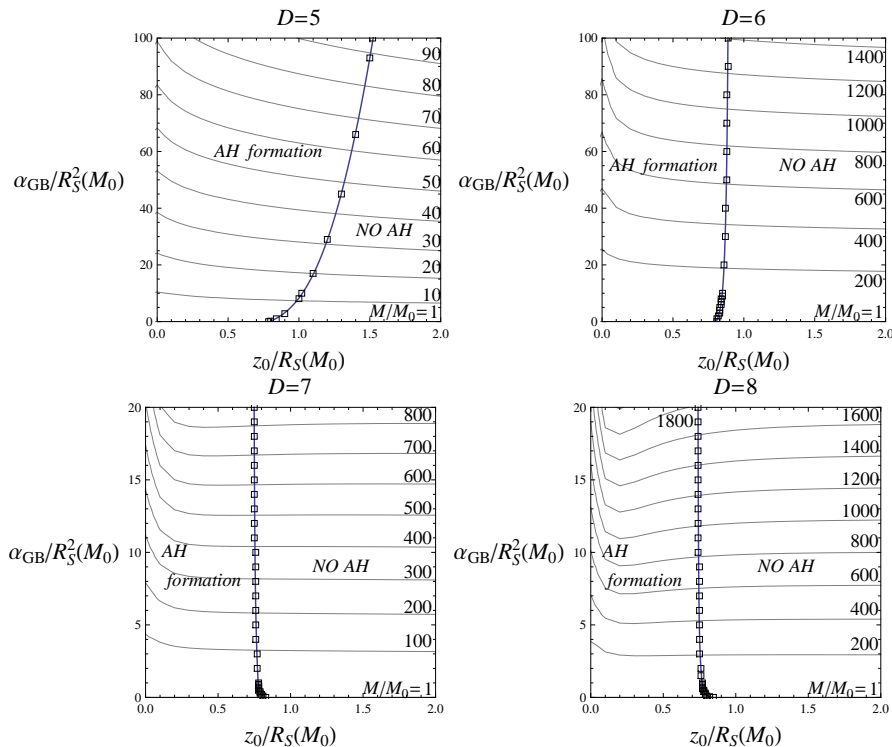


FIG. 7: The regions where the AH can be found (AH formation) and cannot be found (NO AH) and contours of M/M_0 on a $(z_0, \alpha_{\text{GB}})$ plane in the unit $R_S(M_0)$. The AH cannot be found for $z_0 > z_0^{(\text{crit})}$, and numerical data of $z_0^{(\text{crit})}$ are shown by squares (\square). The ADM mass becomes large as α_{GB} is increased.

is the critical value for the AH formation. As the value of z_0 is increased, the AH becomes more distorted. There is the other solution to the AH equation, which corresponds to the inner boundary of the trapped region. At $z_0 = z_0^{(\text{crit})}$, the two solutions degenerate and the solution vanishes for $z_0 > z_0^{(\text{crit})}$.

Figure 7 shows the region where the AH can be found on the $(z_0, \alpha_{\text{GB}})$ plane for $D = 5$ – 8 . Here, the unit of the length is adopted as $R_S(M_0)$. In general dimensions, the AH is not formed for sufficiently large z_0 . In the cases $D = 5$ and 6 , the value of $z_0^{(\text{crit})}/R_S(M_0)$ becomes large as α_{GB} is increased. At first glance, one may think that increasing the coupling constant α_{GB} helps the AH formation. However, this interpretation is not correct, because in this figure, the artificial mass M_0 is used in the length unit $R_S(M_0)$. As we have seen in Sec. IIID, the ADM mass M is changed as α_{GB} is increased following Eq. (26). Several contours of M/M_0 are shown in Fig. 7. As the value of α_{GB} is increased, the mass M also becomes large.

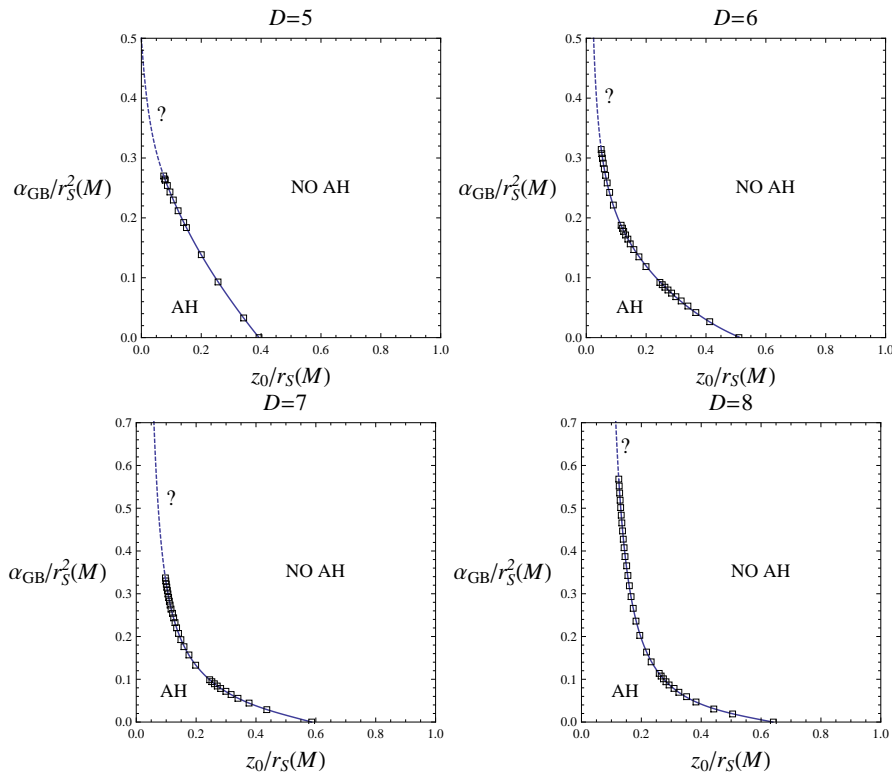


FIG. 8: The regions where the AH can be found (AH) and cannot be found (NO AH) on a $(z_0, \alpha_{\text{GB}})$ plane in the unit $r_S(M)$. The numerical data are shown by squares (\square), and solid line shows the border line of the region of AH formation drawn by interpolation. The dotted line is expected border line for large α_{GB} for which numerical data were not taken. The border line is expected to intersect z_0 axis at $\alpha_{\text{GB}}/r_S^2(M) = 0.5$ in the case $D = 5$, and not to cross the z_0 axis for $D \geq 6$.

Figure 8 shows the region of AH formation on the $(z_0, \alpha_{\text{GB}})$ plane, but now the Schwarzschild radius of the ADM mass, $r_S(M)$, is used as the unit of the length. In all dimensions $D = 5-8$, the value $z_0^{(\text{crit})}$ decreases as the value of α_{GB} is increased, indicating that the coupling constant α_{GB} makes the AH formation difficult compared to the GR case. This is a natural result, because in the spherically symmetric case, the ratio of the horizon radius to the Schwarzschild radius, $r_H(M)/r_S(M)$, decreases as $\alpha_{\text{GB}}/r_S^2(M)$ is increased. The border of the region of the AH formation is shown by a solid curve by interpolating the numerical data. The dashed line shows the expected border for large α_{GB} for which numerical calculation has not been done in this paper. In the case $D = 5$, it is naturally expected that the border line crosses z_0 axis at $\alpha_{\text{GB}}/r_S^2(M) = 0.5$, because for this value, the horizon radius of the spherically-symmetric black hole becomes zero. For the other dimensions, the

border line would not cross z_0 axis, since $r_H(M) > 0$ for arbitrary value of α_{GB} (see Fig. 2).

C. Penrose inequalities

The Penrose inequality in GR,

$$A_{\text{AH}} \leq \Omega_{D-2} [r_S(M)]^{D-2}, \quad (43)$$

conjectures that the AH area is bounded from above by the horizon area of a spherically-symmetric black hole (Schwarzschild-Tangherlini black hole) with the same mass. The reason for this conjecture as follows. If the cosmic censorship holds, an AH is formed in an EH, and since the EH is located outside of the AH, its area is expected to be larger than that of the AH. Because of the area theorem by Hawking, the area of the EH will increase and asymptote to that of a final stationary black hole. Since the horizon area of a rotating black hole is smaller than that of a Schwarzschild black hole with the same mass, and the final mass is smaller than the ADM mass because of the gravitational radiation, the inequality (43) is expected to hold. On the other hand, if the system with an AH whose area is greater than the bound of (43), the validity of the cosmic censorship, one of the assumptions of the above discussion, may be suspected.

The Penrose inequality has been attracting a lot of attentions, and it was proved for momentarily static initial data for $D = 4-7$ [45]. On the other hand, a ‘‘counterexample’’ (but not in a strict sense) has been found in Ref. [50] in a system consisting of combined portions of the Schwarzschild and Oppenheimer-Snyder spacetimes. This example does not contradict the cosmic censorship, but contradicts the assumption that the area of the EH is larger than that of the AH. But the Penrose inequality can be modified to match this counterexample as follows. The AH in a usual sense can be regarded as a ‘‘black hole AH’’ since it is formed in a black hole. On the other hand, we can consider a ‘‘white hole AH’’ formed in a white hole whose past-directed outgoing null geodesic congruence has zero expansion. In the above counterexample, the black hole AH is located inside of the white hole AH, and the area of the white hole AH satisfies the Penrose inequality. Therefore, if we adopt the outermost horizon, the Penrose inequality still holds. This Penrose inequality for the outermost horizon can be proved in spherically-symmetric case assuming weak energy condition [51].

In GB gravity, the relation between the Penrose inequality and the cosmic censorship becomes unclear because the above reasoning for the Penrose inequality may not hold since $-\mathcal{H}_{\mu\nu}$ may violate the energy condition. However, it is still of interest whether the universal relation like (43) holds or not from a mathematical point of view. The proof for the GR case cannot be applied to the GB case at least straightforwardly, because it is unclear if $-\mathcal{H}_{\mu\nu}$ satisfies the energy condition. Therefore, it is interesting to test the inequality using the initial data constructed in this paper.

Other than the original version of the Penrose inequality (43), we can consider another inequality that may be expected to hold in GB gravity.¹ Namely, since the horizon radius $r_H(M)$ of a spherically-symmetric black hole is different from $r_S(M)$, the Penrose inequality may be modified as

$$A_{\text{AH}} \leq \Omega_{D-2} [r_H(M)]^{D-2}, \quad (44)$$

where $r_H(M)$ is defined by Eq. (36). In the following, we test if these two inequalities (43) and (44) hold in our system. For this purpose, we define $P_1 := A_{\text{AH}}/\Omega_{D-2} [r_S(M)]^{D-2}$ and $P_2 := A_{\text{AH}}/\Omega_{D-2} [r_H(M)]^{D-2}$ and evaluate these values for selected values of z_0 and α_{GB} .

Figure 9 shows the behavior of P_1 as a function of z_0 . Here the cases of $\alpha_{\text{GB}} = 0, 1, 10,$ and 100 are shown for $D = 5$ and 6 , and the cases of $\alpha_{\text{GB}} = 0, 0.2, 2, 20$ are shown for $D = 7$ and 8 . In all cases, the values of P_1 are smaller than unity, suggesting that the inequality (43) is kept in this system. We find that P_1 becomes smaller as α_{GB} is increased, and therefore, the coupling constant tends to help the AH satisfy the inequality (43) if α_{GB} is positive.

Figure 10 shows the behavior of P_2 as a function of z_0 . Here the cases of $\alpha_{\text{GB}} = 1, 10,$ and 100 are shown for $D = 5$ and 6 , and the cases of $\alpha_{\text{GB}} = 0.2, 2, 20$ are shown for $D = 7$ and 8 . For all D , the value of P_2 is unity for $z_0 = 0$ because the space agrees with the time-symmetric slice of the spherically symmetric black hole spacetime. As z_0 is increased, the value of P_2 becomes smaller for all values of α . Therefore, the distortion of the AH makes the AH area smaller, and the modified version of the Penrose inequality also holds in our system.

To summarize, the black hole initial data in this paper satisfy both two Penrose inequalities (43) and (44), and no counterexample has been detected. Therefore, the Penrose

¹ The author thanks Tetsuya Shiromizu for this point.

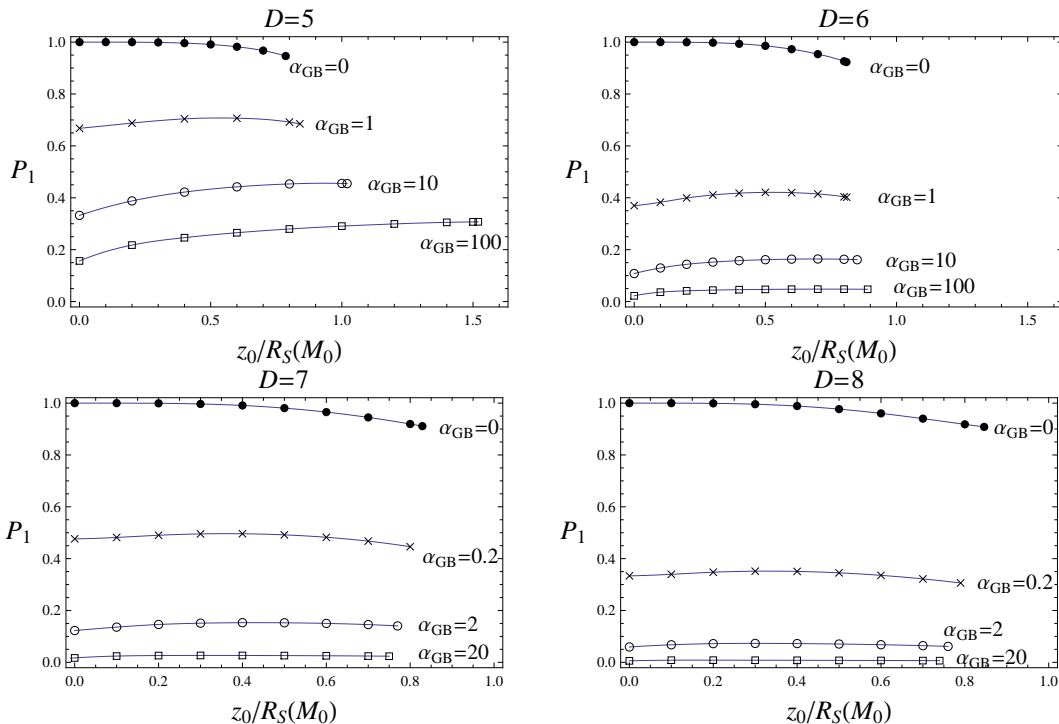


FIG. 9: The behavior of $P_1 := A_{\text{AH}}/\Omega_{D-2}[r_S(M)]^{D-2}$ as a function of z_0 for $\alpha_{\text{GB}} = 0$ (\bullet), 1 (\times), 10 (\circ), and 100 (\square) in the cases $D = 5$ and 6 and for $\alpha_{\text{GB}} = 0$ (\bullet), 0.2 (\times), 2 (\circ), and 20 (\square) in the cases $D = 7$ and 8. The value of P_1 is not greater than unity in all cases, suggesting that the Penrose inequality $P_1 \leq 1$ holds in this system.

inequalities might hold also in GB gravity under appropriate conditions.

VI. SUMMARY AND DISCUSSION

In this paper, we studied the method for generating the initial data for one-black-hole and two-black-hole systems in GB gravity. Assuming the initial space to be momentarily static and conformally flat, the highly nonlinear equation of the Hamiltonian constraint in the $N + 1$ formalism was successfully solved numerically. Using the generated initial data, we studied the common AH that encloses the two black holes, and discussed the Penrose inequalities in GB gravity. The result suggests that both two inequalities (43) and (44) hold in this system.

Here, let us discuss whether the proposed conjecture for the condition of the AH formation in GR can be generalized to GB gravity. In four-dimensional GR, the hoop conjecture

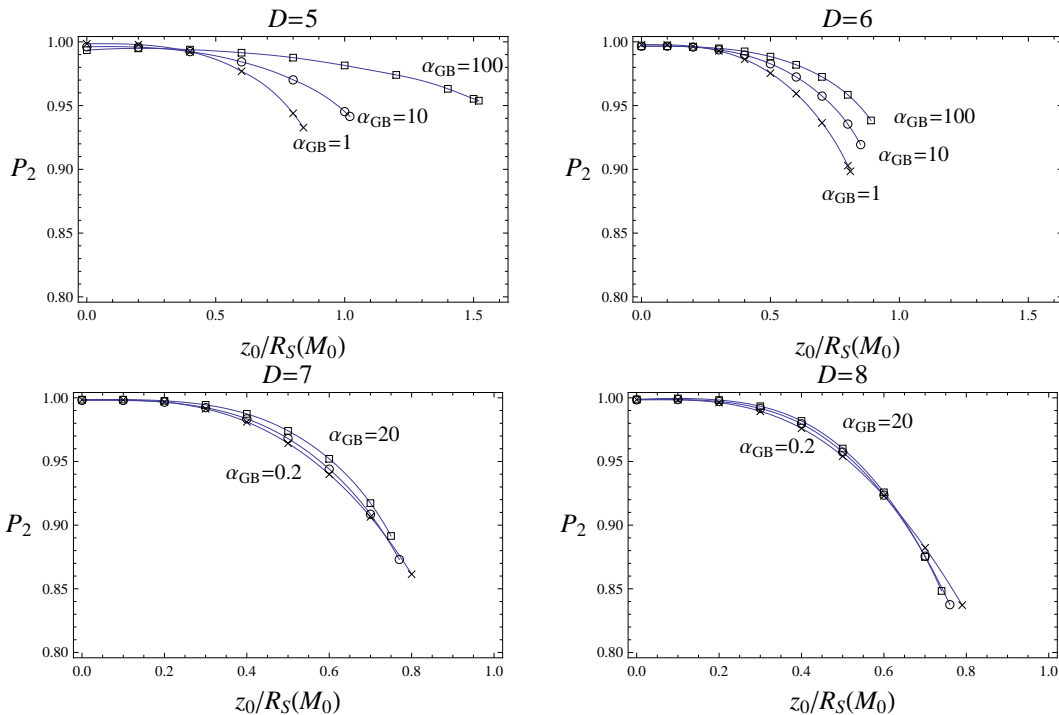


FIG. 10: The behavior of $P_2 := A_{\text{AH}}/\Omega_{D-2}[r_H(M)]^{D-2}$ as a function of z_0 for $\alpha_{\text{GB}} = 1$ (\times), 10 (\circ), and 100 (\square) in the cases $D = 5$ and 6 and for $\alpha_{\text{GB}} = 0.2$ (\times), 2 (\circ), and 20 (\square) in the cases $D = 7$ and 8. The value of P_2 is unity for $z_0 = 0$ and decreases as z_0 is increased. Therefore the modified version of the Penrose inequality $P_2 \leq 1$ also holds in this system.

[52] is well known as the condition of the horizon formation. The hoop conjecture states that a black hole with horizon forms when and only when the hoop length C for a system satisfies $C \lesssim 2\pi r_S(M)$. This conjecture is loosely formulated in the sense that the definitions of the horizon (AH or EH), the hoop, and the mass are not explicitly specified. But this conjecture is known to give the approximate condition of the AH formation (under appropriate definitions of the mass and the hoop which may depend on researchers), although not explicitly proved. The point in this conjecture is that the typical one-dimensional length of the system is restricted from above if an AH is formed, implying that an arbitrarily long AH does not form. But this statement holds only for $D = 4$, because the black hole can be arbitrarily long in higher dimensions as expected from the black string solution, and explicitly shown in [53]. Instead, Ida and Nakao proposed the generalized hoop conjecture [53] as

$$C_{D-3} \lesssim \Omega_{D-3}[r_S(M)]^{D-3}, \quad (45)$$

where C_{D-3} is the typical $(D - 3)$ -dimensional quantity (“hyperhoop”) in this system.

This hyperhoop conjecture was discussed in several papers [42, 53–56], and the results support its effectiveness. Let us consider a two-black-hole system with total mass M , and suppose the two black holes to be momentarily at rest with a typical distance L . In four dimensions, the typical hoop length is estimated by $C \simeq 2\pi r_S(M/2) + 2L$. In a similar manner, in D dimensions, the typical hyperhoop quantity would be $C_{D-3} \simeq \Omega_{D-3}[r_S(M/2)]^{D-3} + \Omega_{D-4}[r_S(M/2)]^{D-4}L$. Substituting this formula into Eq. (45), one has

$$L \lesssim \frac{\Omega_{D-3}}{2^{1/(D-3)}\Omega_{D-4}} r_S(M) \sim r_S(M). \quad (46)$$

This gives an approximate condition for the AH formation at least in a qualitative sense.

Can the hyperhoop conjecture be further extended to GB gravity? One simple manner of generalization would be to change from r_S to r_H in Eq. (45) as

$$C_{D-3} \lesssim \Omega_{D-3}[r_H(M)]^{D-3}, \quad (47)$$

where $r_H(M)$ is defined in Eq. (36). However, this simple generalization does not work for a two-black-hole system. Since the value of C_{D-3} in this case is given by $C_{D-3} \simeq \Omega_{D-3}[r_H(M/2)]^{D-3} + \Omega_{D-4}[r_H(M/2)]^{D-4}L$, the condition (47) gives

$$L \lesssim \left(\frac{\Omega_{D-3}}{\Omega_{D-4}} \right) \frac{[r_H(M)]^{D-3} - [r_H(M/2)]^{D-3}}{[r_H(M/2)]^{D-4}}. \quad (48)$$

Let us consider the case $D = 5$ and suppose α_{GB} and M satisfy the relation $\alpha_{\text{GB}} = (1/2)r_S^2(M/2)$. In this case, $r_H(M/2) = 0$ and $r_H(M) = r_S(M)/\sqrt{2}$, and Eq. (48) gives $L \lesssim \infty$. Therefore, the condition (47) predicts that the common AH forms even for an arbitrarily long distance between the two black holes. This obviously contradicts our numerical result in Fig. 8. Therefore, the condition for the AH formation cannot be obtained at least by a straightforward extension of the hyperhoop conjecture, and a further study is required.

The numerical work in this paper is the first step toward simulations of black holes in GB gravity, and a lot of extensions can be considered. For example, it is necessary to extend our method of generating time-symmetric initial data to the method of generating time-asymmetric initial data like a boosted black hole. For this purpose, the extension of the Bowen-York method [48] should be an interesting possibility. Also, the time evolution of black hole initial data could be done using the approximation analogous to close-limit or close-slow methods in GR [43, 57, 58]. The final goal would be to develop numerically stable formulations of numerical GB gravity by extending $N + 1$ formalism and simulate black hole

systems fully numerically to clarify a lot of interesting phenomena such as time evolution of an unstable GB black hole, rotating systems, and high-velocity collision of black holes.

Acknowledgments

The author thanks Hideo Kodama and Hideki Maeda for helpful discussions that motivated this work. This work was supported by the Grant-in-Aid for Scientific Research (A) (22244030).

-
- [1] N. Arkani-Hamed, S. Dimopoulos and G. R. Dvali, Phys. Lett. B **429**, 263 (1998) [arXiv:hep-ph/9803315].
 - [2] I. Antoniadis, N. Arkani-Hamed, S. Dimopoulos and G. R. Dvali, Phys. Lett. B **436**, 257 (1998) [arXiv:hep-ph/9804398].
 - [3] L. Randall and R. Sundrum, Phys. Rev. Lett. **83**, 3370 (1999) [arXiv:hep-ph/9905221].
 - [4] T. Banks and W. Fischler, arXiv:hep-th/9906038.
 - [5] S. Dimopoulos and G. Landsberg, Phys. Rev. Lett. **87**, 161602 (2001) [arXiv:hep-ph/0106295].
 - [6] S. B. Giddings and S. Thomas, Phys. Rev. D **65**, 056010 (2002) [arXiv:hep-ph/0106219].
 - [7] P. Kanti, Lect. Notes Phys. **769**, 387 (2009) [arXiv:0802.2218 [hep-th]].
 - [8] V. Khachatryan *et al.* [CMS Collaboration], arXiv:1012.3375 [hep-ex].
 - [9] H. Yoshino and M. Shibata, Phys. Rev. D **80**, 084025 (2009) [arXiv:0907.2760 [gr-qc]].
 - [10] M. Zilhao, H. Witek, U. Sperhake, V. Cardoso, L. Gualtieri, C. Herdeiro and A. Nerozzi, Phys. Rev. D **81**, 084052 (2010) [arXiv:1001.2302 [gr-qc]].
 - [11] E. Sorkin, Phys. Rev. D **81**, 084062 (2010) [arXiv:0911.2011 [gr-qc]].
 - [12] L. Lehner and F. Pretorius, Phys. Rev. Lett. **105**, 101102 (2010) [arXiv:1006.5960 [hep-th]].
 - [13] H. Witek, M. Zilhao, L. Gualtieri, V. Cardoso, C. Herdeiro, A. Nerozzi and U. Sperhake, Phys. Rev. D **82**, 104014 (2010) [arXiv:1006.3081 [gr-qc]].
 - [14] H. Witek, V. Cardoso, L. Gualtieri, C. Herdeiro, U. Sperhake and M. Zilhao, arXiv:1011.0742 [gr-qc].
 - [15] M. Shibata and H. Yoshino, Phys. Rev. D **81**, 021501 (2010) [arXiv:0912.3606 [gr-qc]].
 - [16] M. Shibata and H. Yoshino, Phys. Rev. D **81**, 104035 (2010) [arXiv:1004.4970 [gr-qc]].

- [17] C. Lanczos, *Ann. Math.* **39**, 842 (1938).
- [18] D. Lovelock, *J. Math. Phys.* **12**, 498 (1971).
- [19] B. Zwiebach, *Phys. Lett. B* **156**, 315 (1985).
- [20] M. J. Duff, B. E. W. Nilsson and C. N. Pope, *Phys. Lett. B* **173**, 69 (1986).
- [21] D. J. Gross and J. H. Sloan, *Nucl. Phys. B* **291**, 41 (1987).
- [22] S. Ogushi and M. Sasaki, *Prog. Theor. Phys.* **113**, 979 (2005) [arXiv:hep-th/0407083].
- [23] A. Buchel, J. Escobedo, R. C. Myers, M. F. Paulos, A. Sinha and M. Smolkin, *JHEP* **1003**, 111 (2010) [arXiv:0911.4257 [hep-th]].
- [24] Y. P. Hu, H. F. Li and Z. Y. Nie, *JHEP* **1101**, 123 (2011) [arXiv:1012.0174 [hep-th]].
- [25] D. G. Boulware and S. Deser, *Phys. Rev. Lett.* **55**, 2656 (1985).
- [26] T. Torii and H. Maeda, *Phys. Rev. D* **71**, 124002 (2005) [arXiv:hep-th/0504127].
- [27] T. Torii and H. Maeda, *Phys. Rev. D* **72**, 064007 (2005) [arXiv:hep-th/0504141].
- [28] D. L. Wiltshire, *Phys. Rev. D* **38**, 2445 (1988).
- [29] C. Charmousis and J. F. Dufaux, *Class. Quant. Grav.* **19**, 4671 (2002) [arXiv:hep-th/0202107].
- [30] R. Zegers, *J. Math. Phys.* **46**, 072502 (2005) [arXiv:gr-qc/0505016].
- [31] G. Dotti and R. J. Gleiser, *Class. Quant. Grav.* **22**, L1 (2005) [arXiv:gr-qc/0409005].
- [32] G. Dotti and R. J. Gleiser, *Phys. Rev. D* **72**, 044018 (2005) [arXiv:gr-qc/0503117].
- [33] R. J. Gleiser and G. Dotti, *Phys. Rev. D* **72**, 124002 (2005) [arXiv:gr-qc/0510069].
- [34] M. Beroiz, G. Dotti and R. J. Gleiser, *Phys. Rev. D* **76**, 024012 (2007) [arXiv:hep-th/0703074].
- [35] T. Takahashi and J. Soda, arXiv:1008.1618 [gr-qc].
- [36] Y. Brihaye, B. Kleihaus, J. Kunz and E. Radu, *JHEP* **1011**, 098 (2010) [arXiv:1010.0860 [hep-th]].
- [37] V. S. Rychkov, *Phys. Rev. D* **70**, 044003 (2004) [arXiv:hep-ph/0401116].
- [38] T. Torii and H. A. Shinkai, *Phys. Rev. D* **78**, 084037 (2008) [arXiv:0810.1790 [gr-qc]].
- [39] M. Shibata and T. Nakamura, *Phys. Rev. D* **52**, 5428 (1995).
- [40] T. W. Baumgarte and S. L. Shapiro, *Phys. Rev. D* **59**, 024007 (1998) [arXiv:gr-qc/9810065].
- [41] D. R. Brill and R. W. Lindquist, *Phys. Rev.* **131**, 471 (1963).
- [42] H. Yoshino and Y. Nambu, *Phys. Rev. D* **70**, 084036 (2004) [arXiv:gr-qc/0404109].
- [43] H. Yoshino, T. Shiromizu and M. Shibata, *Phys. Rev. D* **72**, 084020 (2005) [arXiv:gr-qc/0508063].
- [44] R. Penrose, *Ann. New York Acad. Sci.* **224**, 125 (1973).

- [45] H. L. Bray and D. A. Lee, arXiv:0705.1128 [math.DG].
- [46] S. S. Chern, Ann. Math. **48**, 674 (1945).
- [47] S. Brandt and B. Brügmann, Phys. Rev. Lett. **78**, 3606 (1997) [arXiv:gr-qc/9703066].
- [48] J. M. Bowen and J. W. York, Jr, Phys. Rev. D **21**, 2047 (1980).
- [49] M. Nozawa and H. Maeda, Class. Quant. Grav. **25**, 055009 (2008) [arXiv:0710.2709 [gr-qc]].
- [50] I. Ben-Dov, Phys. Rev. D **70**, 124031 (2004) [arXiv:gr-qc/0408066].
- [51] E. Malec and N. Ó Murchadha, Phys. Rev. D **49**, 6931 (1994) [arXiv:gr-qc/9401014].
- [52] K. S. Thorne, in *Magic without Magic: John Archbald Wheeler*, edited by J.Klauder (Freeman, San Francisco, 1972).
- [53] D. Ida and K.-i. Nakao, Phys. Rev. D **66**, 064026 (2002).
- [54] H. Yoshino and Y. Nambu, Phys. Rev. D **67**, 024009 (2003).
- [55] C. M. Yoo, K. I. Nakao and D. Ida, Phys. Rev. D **71**, 104014 (2005) [arXiv:gr-qc/0503008].
- [56] Y. Yamada and H. a. Shinkai, Class. Quant. Grav. **27**, 045012 (2010) [arXiv:0907.2570 [gr-qc]].
- [57] R. H. Price and J. Pullin, Phys. Rev. Lett. **72**, 3297 (1994) [arXiv:gr-qc/9402039].
- [58] H. Yoshino, T. Shiromizu and M. Shibata, Phys. Rev. D **74**, 124022 (2006) [arXiv:gr-qc/0610110].